Polyelectrolyte Multilayers Assembled Entirely from Immune Signals on Gold Nanoparticle Templates Promote Antigen-Specific T Cell Response

Peipei Zhang,[†] Yu-Chieh Chiu,[†] Lisa H. Tostanoski,[†] and Christopher M. Jewell[*,†,‡,§]

[†]Fischell Department of Bioengineering, University of Maryland, College Park, Maryland 20742, United States, [‡]Department of Microbiology and Immunology, University of Maryland School of Medicine, Baltimore, Maryland 21201, United States, and [§]Marlene and Stewart Greenebaum Cancer Center, Baltimore, Maryland 21201, United States

ABSTRACT Materials that allow modular, defined assembly of immune signals could support a new generation of rationally designed vaccines that promote tunable immune responses. Toward this goal, we have developed the first polyelectrolyte multilayer (PEM) coatings built entirely from immune signals. These immune-PEMs (iPEMs) are self-assembled on gold nanoparticle templates through stepwise electrostatic interactions between peptide antigen and polyanionic toll-like receptor (TLR) agonists that serve as molecular adjuvants. iPEMs do not require solvents or mixing, offer direct control over the composition and loading of vaccine components, and can be coated on substrates at any scale. These films also do not require other structural components, eliminating the potentially confounding effects caused by the inherent immune-stimulatory characteristics of many synthetic polymers. iPEM loading on gold nanoparticle substrates is tunable, and cryoTEM reveals iPEM shells coated on gold cores. These nanoparticles are efficiently internalized by primary dendritic cells (DCs), resulting in activation, selective triggering of TLR signaling, and presentation of the antigens used to assemble iPEMs. In coculture, iPEMs drive antigen-specific T cell proliferation and effector cytokines but not cytokines associated with more generalized inflammation. Compared to mice treated with soluble antigen and adjuvant, iPEM immunization promotes high levels of antigen-specific $CD8^+$ T cells in peripheral blood after 1 week. These enhancements result from increased DC activation and antigen presentation in draining lymph nodes. iPEM-immunized mice also exhibit a potent recall response after boosting, supporting the potential of iPEMs for designing well-defined vaccine coatings that provide high cargo density and eliminate synthetic film components.

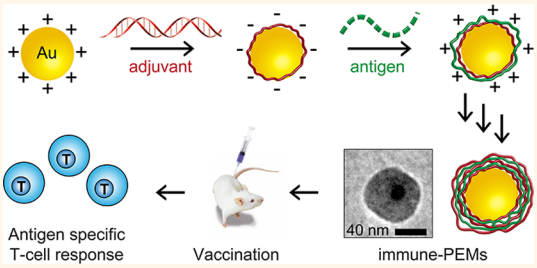

KEYWORDS: vaccine · polyelectrolyte multilayer · gold nanoparticle · immunology · nanotechnology · adjuvant · immunotherapy

New vaccines that promote efficient immune responses while directing the specific characteristics of these responses—T cell *versus* antibody response, for example—could help address challenges in areas from infectious disease to cancer. Controlling immunity at this level depends on integration of the combinations, doses, and intervals over which antigens and adjuvants are received and processed in lymph nodes (LNs) or the spleen.[1,2] Toward this new level of control, biomaterials have been intensely studied because these materials offer advantages such as controlled release, targeting, and cargo protection.[3−5] However, some of the persistent challenges facing materials-based vaccines are the intrinsic inflammatory properties of many polymers, the inability to control the combinations of signals that are delivered in a modular fashion, the solvents and high-energy processes required for manufacturing, and the relatively low loading levels of cargo (*e.g.*, antigen encapsulated in degradable particles). To help address these challenges, we used gold nanoparticles (AuNPs) as a template for layer-by-layer (LbL) assembly of the first polyelectrolyte multilayer (PEM) films assembled entirely from immune signals (*e.g.*, antigens, adjuvants).

PEMs are self-assembled, nanoscale structures built through electrostatic or hydrophobic interactions occurring during LbL deposition of film components.[6−9] These

* Address correspondence to cmjewell@umd.edu.

Received for review April 10, 2015 and accepted June 2, 2015.

Published online June 02, 2015
10.1021/acsnano.5b02153

films allow control over the combinations and relative concentrations of polyelectrolytes assembled on substrates at nano-, micro-, or macroscales.[9−12] The robust properties of PEMs have motivated their use in biomedical applications ranging from drug and nucleic acid delivery to radiotherapy and vaccination.[7,13,14] In the vaccine field, synthetic polymers have been used to encapsulate or incorporate antigens and toll-like receptor agonists (TLRa) into PEMs coated on microneedles for transdermal delivery and on particles or in hollow capsules for injection.[8,9,15−17] Common polymers incorporated to build these vaccine particles include dextran sulfate (DS), poly(sodium styrenesulfonate) (PSS), poly(L-glutamic acid) (PGA), poly(allylamine hydrochloride) (PAH), poly(L-lysine) (PLL), and poly(L-arginine) (PLA). These PEM structures can enhance dendritic cell (DC) and T cell function. For example, model antigen (ovalbumin, OVA) or clinically relevant antigens (*e.g.*, HIV/SIV) can be encapsulated within a PEM shell composed of poly(methacrylic acid) and poly(vinylpyrrolidone) to increase DC uptake and activation, resulting in expansion of antigen-specific T cells in a coculture.[18,19] PEM capsules formed from DS and PLA have been used to encapsulate influenza or OVA antigens.[20] Immunization of mice with these materials provides protection against respective challenges with flu or B16-F10 tumors expressing OVA.[20] Strategies that exploit PEMs but offer new features, such as increased cargo density or better vaccine definition, could improve vaccine design and performance.

AuNPs have been widely studied in nanomedicine because AuNPs are immunologically inert, nontoxic, and can be readily synthesized with well-controlled properties (*e.g.*, diameter).[21−24] These characteristics are particularly well-suited to study and enhance vaccination.[25] For example, monodispersed AuNPs have been used to measure particle trafficking to resident immune cells in LNs—the tissues that coordinate immune function.[26] In a therapeutic context, AuNPs have been modified with tissue-specific antigens or tolerogenic drugs to study immunotherapies for cancer or autoimmune diseases.[27,28] Another area in which AuNPs have been exploited is the study of intrinsic immune function of synthetic materials.[29] In these studies, the surfaces of AuNPs were functionalized with defined chemical groups to systematically vary hydrophobicity, and these changes were linked to changes in inflammatory function in cells and mice.[29] Intrinsic immune effects are of particular relevance to new materials-based vaccines, as several studies with important biomaterials, such as poly(lactide-*co*-glycolide) and polystyrene, have revealed that these polymers can activate innate immune pathways (*e.g.*, inflammasomes) and polarize adaptive immune response even in the absence of other adjuvants.[30−32] This finding suggests that the intrinsic immune-stimulatory capabilities of polymers might complicate rational design of new vaccines because the carrier itself can alter, amplify, or suppress the response to other antigens or adjuvants included in vaccines. Thus, new materials that leverage the properties of PEMs but eliminate the intrinsic immune effects of synthetic polymers might offer new routes to rational vaccine design and contribute to more programmable immune responses.

While PEMs have been used to modify the surfaces of AuNPs for drug delivery,[33−35] these two technologies have not been combined in vaccination or immunotherapy. We hypothesized that inert AuNP templates coated with PEMs built entirely from immune signals might serve as a platform for designing modular vaccines with high signal densities and without the potentially confounding effects associated with the intrinsic immune characteristics of polymeric carriers. These immune-PEMs (iPEMs) were assembled on AuNPs (iPEM-AuNPs) by alternate deposition of polyinosinic−polycytidylic acid (polyIC)—a nucleic acid TLR agonist that exhibits potent adjuvant properties—and either SIINFEKL peptide antigen (SIIN, zwitterionic) or SIINFEKL modified with nona-arginine (SIIN*) to serve as a cationic "anchor" (Figure 1). In addition to supporting film growth, nona-arginine is a potent cell-penetrating peptide that enhances cell uptake of associated cargo.[36] Thus, iPEM formation draws on the adjuvant component (*i.e.*, polyIC) to provide negative

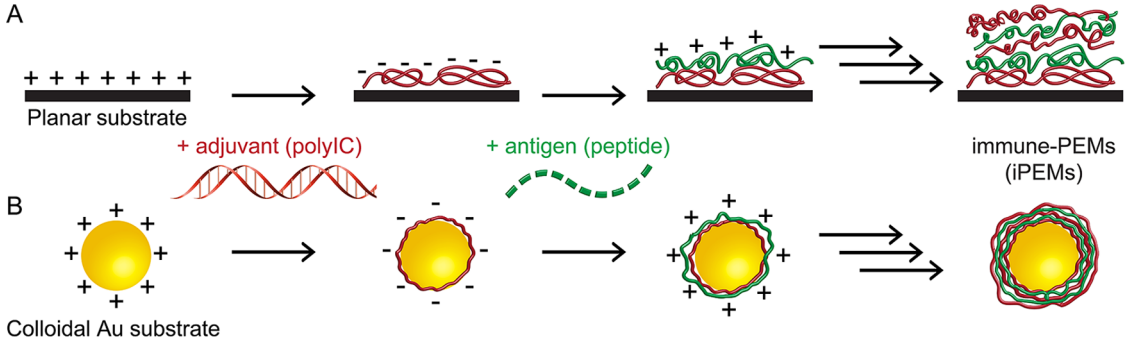

Figure 1. Schematic depiction of a layer-by-layer approach to assemble immune-PEMs (iPEMs) from adjuvants and antigens on (A) planar or (B) gold nanoparticle substrates.

charge for electrostatic interactions with peptide components (*i.e.*, SIIN*, SIIN). iPEM assembly is carried out using an all-aqueous, LbL process that does not require solvents, mixing, heating, or refrigeration employed with many materials. The LbL assembly process also provides direct control over the combinations and concentrations of adjuvants and antigens used to build iPEMs by adjusting the number of cycles. A characteristic PEM shell develops on AuNP cores as PEM layers are deposited, and because iPEMs are composed entirely of immune signals, the loading levels are very high relative to many other particle delivery systems. Further, iPEM coatings juxtapose the immune signals, providing better control over the delivery of multiple cargos to support immune polarization.

In culture, DCs incubated with iPEM-coated AuNPs are efficiently internalized. These cells exhibit high levels of activation, expand antigen-specific T cells during coculture, and induce secretion of effector cytokines. Intradermal (i.d.) immunization of mice with iPEMs increases antigen presentation and DC activation in draining LNs, induces high levels of circulating antigen-specific $CD8^+$ T cells, and promotes rapid recall responses. Importantly, compared to simple mixtures of peptide and adjuvant, iPEMs drive significantly higher frequencies of antigen-specific $CD8^+$ T cells. These findings suggest that iPEMs could support a modular, LbL-based approach for rational design of vaccines using immune signals that serve as structural components and as signals to actively direct immune response.

RESULTS

Assembly and Characterization of iPEM-AuNPs. To determine if PEMs could be assembled from polyIC (anionic) and SIIN (zwitterionic) or SIIN* (cationic), films were first deposited on planar silicon substrates by LbL deposition (Figure 1A). iPEMs composed of polyIC and SIIN* grew linearly (R^2 = 0.999) at a rate of 10.1 nm/per bilayer, reaching a thickness of 43.5 ± 2.2 nm after four bilayers (Figure 2A). In contrast, film thickness did not increase when silicon substrates were alternatingly exposed to solutions of polyIC and SIIN using the same cargo concentrations and number of deposition cycles (Figure 2A). Similar results were obtained during LbL deposition on quartz substrates to measure cargo loading, with a linear increase in antigen (Figure 2B, $R^2 = 0.984$) and adjuvant (Figure 2C, $R^2 = 0.993$) loading observed during assembly of $(polyIC/SIIN^*)_4$ but not when substrates were exposed to solutions of polyIC and SIIN. Using fluorescently labeled vaccine components (Cy5-polyIC, FITC-SIIN*), both polyIC and SIIN* could be visualized by fluorescence microscopy following removal of a portion of the film with a needle to provide contrast (Figure 2D). These results indicate that the increased cationic charge conferred by R_9 facilitates linear growth of iPEMs assembled from adjuvant and peptide antigen. This general approach was next adapted to deposit iPEMs on injectable colloidal substrates for subsequent use in cell and animal studies.

To prepare iPEM-coated particles, polyIC/SIIN* films were deposited on AuNP templates, as illustrated in Figure 1B. After each exposure to polyIC or SIIN*, NPs were collected by centrifugation and washed before exposure to the next layer. The uncoated AuNP templates exhibited a diameter of 16 ± 4 nm, as confirmed by dynamic light scattering (Figure 3A). Particle diameter increased during deposition of each successive PEM bilayer, with AuNP-$(polyIC/SIIN^*)_1$, AuNP-$(polyIC/SIIN^*)_2$, and AuNP-$(polyIC/SIIN^*)_3$ exhibiting diameters of 49 ± 14, 91 ± 30, and 176 ± 29 nm, respectively (Figure 3A). Film growth on AuNPs was further confirmed by measuring the ζ-potential, which oscillated between negative and positive values with each adsorption step of polyIC and SIIN*, respectively (Figure 3B). The LbL nature of this growth also allowed linear control over the amounts of the immune signals coated onto the AuNP templates. As the number of bilayers was increased from 0 to 3, polyIC loading on AuNPs reached 60.7, 104.1, and 158.8 μg/mg of AuNP, respectively, while the respective peptide loading reached 31.9, 64.9, and 90.2 μg/mg of AuNP (Figure 3C). Over these same cycles, corresponding

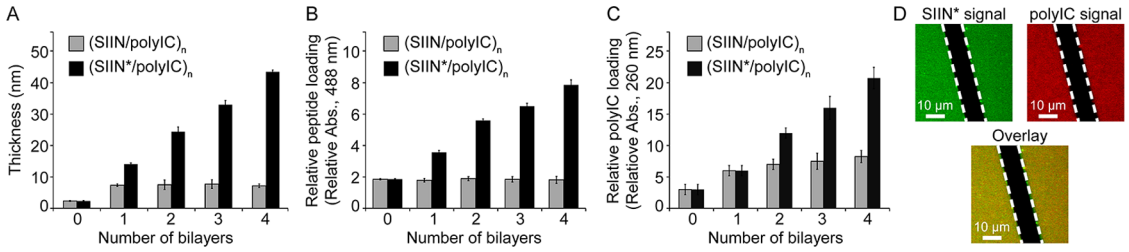

Figure 2. iPEMs can be assembled on planar substrates with linear control over growth and loading of peptide antigens and molecular TLR agonists as adjuvants. iPEMs were assembled on quartz or silicon substrates using $(polyIC/SIIN)_n$ or $(polyIC/SIIN^*)_n$ with $n = 0-4$. (A) Thickness of iPEM films on silicon substrates measured by ellipsometry as a function of the number of layers deposited. Relative loading of (B) peptide antigen and (C) polyIC adjuvant on quartz substrates using FITC-labeled SIIN or SIIN* and Cy5-labeled polyIC. (D) Film components were visualized by fluorescence microscopy. Peptide (green signal), polyIC (red signal), and overlay (yellow signal) images are shown after removing a portion of the film with a needle to provide contrast (dashed lines).

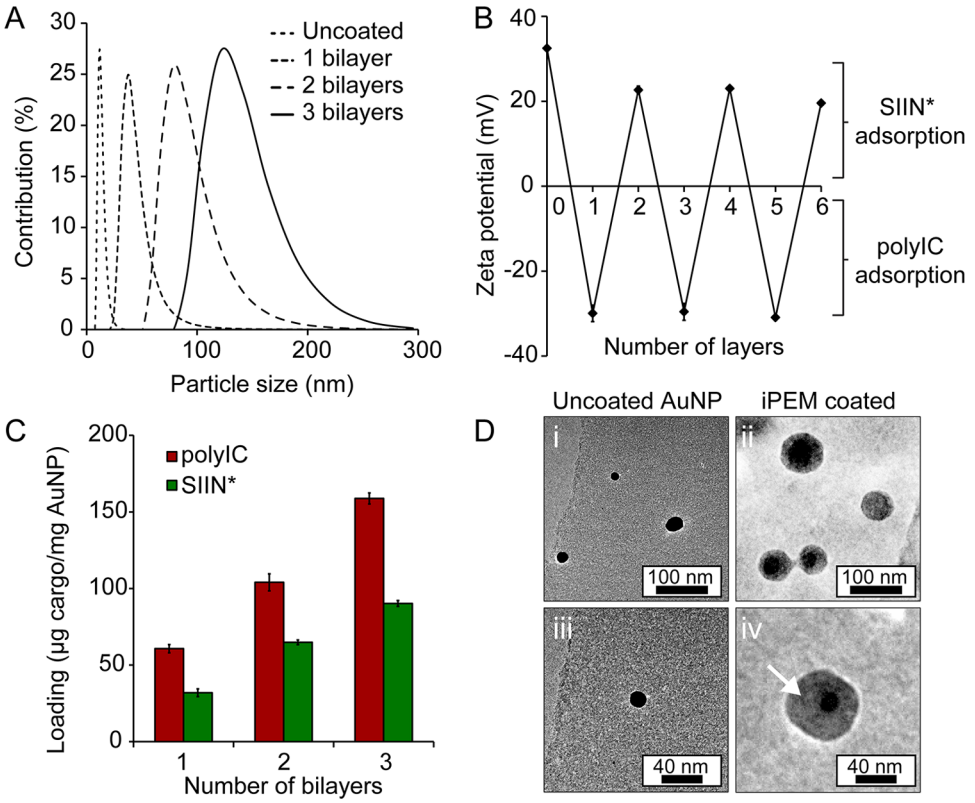

Figure 3. iPEMs assembled on AuNP substrates provide control over vaccine cargo loading and exhibit a core−shell structure. (A) Diameter of iPEM particles measured by dynamic light scattering as a function of the number of layers deposited. (B) Inversion of ζ-potential of iPEMs on AuNPs as successive layers of cationic antigen and anionic adjuvant are adsorbed. (C) Linear control over the loading of peptide antigen (SIIN*) and polyIC during deposition of three bilayers (six layers). (D) CryoTEM images of (i,iii) uncoated and (ii,iv) iPEM-coated AuNP cores at low (i,ii) and high (iii,iv) magnification. The arrow in (iv) indicates an iPEM shell surrounding the AuNP core.

decreases in cargo concentration were observed in the solutions used to deposit each iPEM layer (Supporting Information Figure S1).

To visualize iPEMs coated on the templates, we characterized uncoated AuNPs and AuNP-(polyIC/SIIN*)$_2$ using cryogenic transmission electronic microscopy (cryoTEM). These experiments revealed defined, spherical AuNP cores prior to coating with iPEMs (Figure 3D,i,iii). After film deposition, iPEM particles exhibited a characteristic core−shell structure (Figure 3D,ii,iv), with dark regions indicating AuNP cores surrounded by thicker, more diffuse iPEM shell regions (Figure 3D,iv, arrow). While most iPEM-coated particles were individually dispersed, we observed a subset of the population clustered in groups of two or three particles (Figure S2A). To explore particle stability and dispersion in a setting relevant to physiologic conditions, we incubated iPEM-AuNPs in serum-free medium or serum-rich medium at 37 °C. Over the duration of the study (24 h), we observed no significant changes in the sizes of particles incubated in serum-free medium, whereas particle size gradually increased to 200−300 nm over 24 h when incubated in serum-rich medium (Figure S2B). Together, these data indicate that iPEMs can be self-assembled on AuNPs with tunable cargo loading, and that these particles maintain sizes useful for vaccination even when incubated at elevated temperature in the presence of high concentrations of serum.

iPEM-AuNP Vaccines Are Efficiently Internalized by Antigen-Presenting Cells. We next assessed uptake of iPEM vaccine particles by treating splenic DCs (CD11c$^+$) with AuNP-(polyIC/SIIN*)$_2$ prepared from fluorescently labeled peptide and adjuvant. Following incubation, confocal microscopy revealed high levels of peptide (green signal) and polyIC (red signal) located within cells (Figure 4A). These signals were punctate throughout the extranuclear region and exhibited a high degree of colocalization between polyIC and peptide, indicating juxtaposition and co-delivery of both vaccine components. In similar studies, flow cytometry was used to quantitatively assess the interactions of iPEM-AuNPs with DCs. iPEM-coated NPs efficiently associated with DCs in a dose-dependent manner, with nearly all cells positive for both iPEM components (*i.e.*, polyIC, SIIN*) at low dilution factors (Figure 4B,C). Association of peptide and adjuvant in iPEM form with cells was much greater than levels observed in cells treated with equivalent doses in soluble form (Figure 4B,C). Further, the viability of DCs treated with iPEM-coated AuNPs was 91.3% relative to cells treated with a TLR4 agonist (lipopolysaccharide, LPS). This level was statistically equivalent to the viability

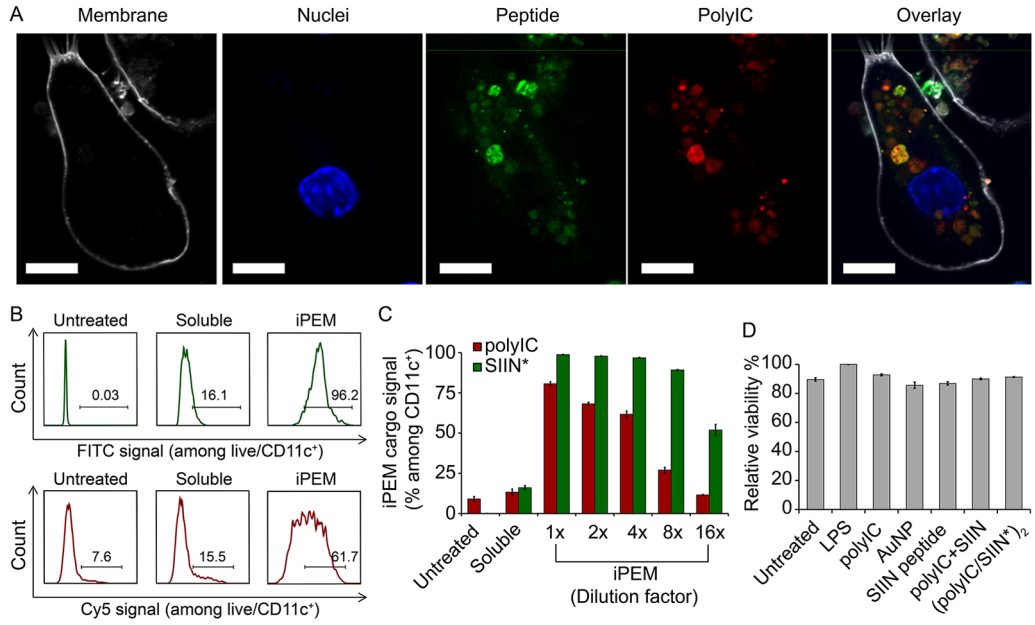

Figure 4. iPEM-AuNPs are internalized by DCs without toxicity and activate TLR3 signaling. (A) Confocal microscopy images demonstrating the cytosolic distribution of polyIC and SIIN* in primary DCs following a 3 h incubation with iPEMs using a structure of AuNP-(SIIN*/polyIC)$_2$. The panels indicate the cell membrane (white), nucleus (blue), SIIN* peptide (green), polyIC adjuvant (red), and the overlay (right most image); scale bars are 10 μm. (B) Representative flow cytometry histograms illustrating association of peptide (FITC, green) and polyIC (Cy5, red) with primary DCs. Cells were untreated (left), incubated with soluble peptide and polyIC (center), or incubated with iPEM (right). (C) Quantitative analysis of peptide and polyIC association with DCs based on the gates shown in (B). Soluble formulations correspond to a dose equivalent to that of the iPEM formulation shown at the 4× dilution. (D) Relative viability of DCs following incubation normalized to DCs treated with LPS. PolyIC + SIIN indicates cells treated with a simple mixture of peptide and polyIC.

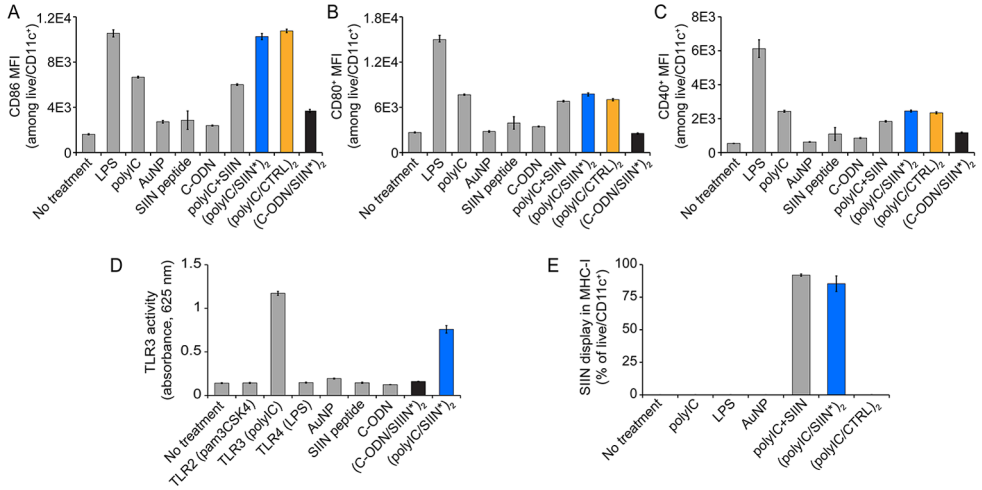

Figure 5. iPEMs activate DCs, trigger TLR3 signaling, and promote presentation of SIIN peptide. Splenic CD11c$^+$ DCs from B6 mice were incubated for 18 h with the indicated formulations, then flow cytometry was used to assess the expression of (A) CD86, (B) CD80, and (C) CD40. (D) TLR3 signaling in HEK-Blue TLR3 cells following a 16 h incubation. PolyIC was included as a positive control, and TLR2 and TLR4 agonists were included as negative selectivity controls. C-ODN indicates a non-immunogenic control oligonucleotide. (E) Presentation of SIIN peptide as measured by flow cytometry following staining with an antibody that binds SIINFEKL only when presented *via* the MHC-I. For panels (A−C,E), (polyIC/CTRL)$_2$ indicates iPEMs assembled from polyIC and a control peptide that is unable to be bound by anti-SIIN/MHC-I.

of DCs treated with soluble polyIC (92.8%) or a mixture of soluble polyIC and peptide (90.0%) (Figure 4D). These results demonstrate that iPEMs assembled from polyIC and SIIN* on AuNPs are efficiently internalized by primary DCs without significant toxicity.

iPEM-AuNPs Promote Selective TLR Signaling and Efficiently Activate DCs. To determine if iPEMs stimulate DC function, splenic DCs were incubated with AuNP-(polyIC/SIIN*)$_2$. Expression of classical DC activation markers and TLR3 signaling were then measured, along with presentation of SIINFEKL peptide *via* major histocompatibility complex I (MHC-I). DCs treated with iPEM-coated AuNPs exhibited high levels of CD40 expression that were comparable to those observed in DCs treated

with soluble LPS (TLR4 agonist) or polyIC (TLR3 agonist) that served as positive controls (Figure 5A). These levels were also similar to those observed in cells treated with equivalent, soluble doses of polyIC and SIIN. Treatment of DCs with uncoated AuNPs resulted in baseline activation levels equal to those observed in untreated DCs (Figures 5A and S2). Analogous trends were observed in the expression levels of CD86 (Figures 5B and S3) and CD80 (Figures 5C and S3). For each marker, the level of activation could be increased or decreased by increasing or decreasing the number of layers—and therefore, dose—used to assemble iPEMs (Supporting Information Figure S4A–C). To test if the immunostimulatory properties of iPEMs result, in part, from formulation of antigen into a particulate form, AuNPs were coated with control iPEMs assembled from polyIC and a second peptide (CTRL) to form AuNP-(polyIC/CTRL)$_2$ or with SIIN* and a non-immunostimulatory control oligonucleotide (C-ODN) to form AuNP-(C-ODN/SIIN*)$_2$. For each activation marker, DCs treated with AuNP-(polyIC/CTRL)$_2$ drove DC activation levels similar to those observed in DCs treated with AuNP-(polyIC/SIIN*)$_2$ (Figure 5A–C, orange *vs* blue). In contrast, treatment with AuNP-(C-ODN/SIIN*)$_2$ did not activate DCs, as indicated by mean fluorescent intensities (MFIs) similar to the low values observed in cells treated with AuNPs or free C-ODN or in untreated cells. Thus, the immunogenicity of iPEMs results from juxtaposition of antigens and adjuvants, not simply from formulating antigen into a particle (Figure 5A–C, black *vs* blue).

In addition to surface activation markers, treatment of DCs with iPEMs formed from polyIC and SIIN* also efficiently and specifically activated TLR3 signaling. These effects were selective to TLR3, as a lack of signal was observed in cells treated with negative controls of Pam3CSK4 (TLR2 agonist) or LPS (TLR4 agonist)—agonists recognized by TLR pathways that are activated by molecular patterns not based on the dsRNA (Figure 5D). Importantly, activation was also specific, as TLR3 activity was not observed in cells treated with AuNPs coated with iPEMs prepared from C-ODN and SIIN* (AuNP-(ODN/SIIN*)$_2$). Together, these results demonstrate that iPEMs coated on AuNPs activate DCs without dependence on the peptide sequence incorporated into the iPEMs. Further, the incorporation of adjuvants (*e.g.*, TLR3 agonists) into iPEMs does not impact the potency, selectivity, or specificity of these vaccine components. Similar questions of selectivity and specificity were next asked regarding the antigen component of iPEMS.

iPEM-AuNPs Promote Selective Antigen Presentation of Antigens Used To Assemble iPEMs. To determine if antigen used to build iPEMs is processed and presented by DCs, splenic DCs were treated with AuNP-(polyIC/SIIN*)$_2$ or AuNP-(polyIC/CTRL)$_2$ as above. The cells were then stained with an antibody that binds SIINFEKL peptide when presented in the context of MHC-I—a pathway important in promoting cell-mediated immune responses against intracellular pathogens such as viruses. In these studies, 85.4% ± 5.9% of DCs treated with

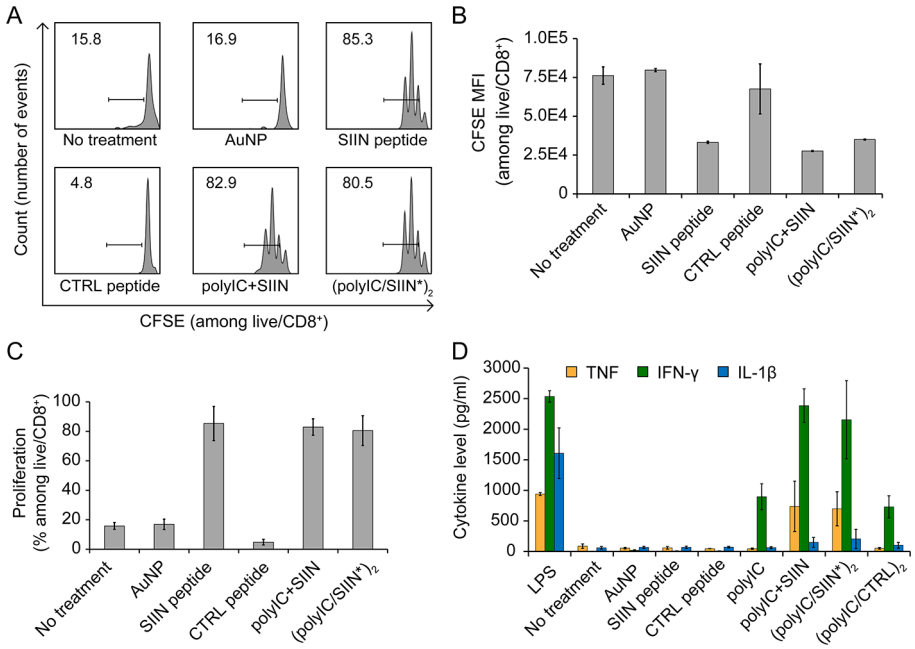

Figure 6. DCs treated with iPEMs drive proliferation of CD8$^+$ antigen-specific T cells in coculture. (A) Histogram depicting division and proliferation in OT-1 T cells labeled with CFSE prior to coculture with DCs incubated with the indicated formulations for 48 h (see Methods). Cocultures were carried out for 48 h. (B) Mean fluorescence intensity (MFI) of CFSE levels of the T cells described in (A). (C) Frequency of T cells that proliferated based on the gates shown in (A). (D) ELISA analysis of IFN-γ, TNF, and IL-1β production in the supernatant of the cocultures described in (A–C). Supernatants were collected 48 h after coculture. For all panels, CTRL refers to an irrelevant control peptide not recognized by OT-1 cells.

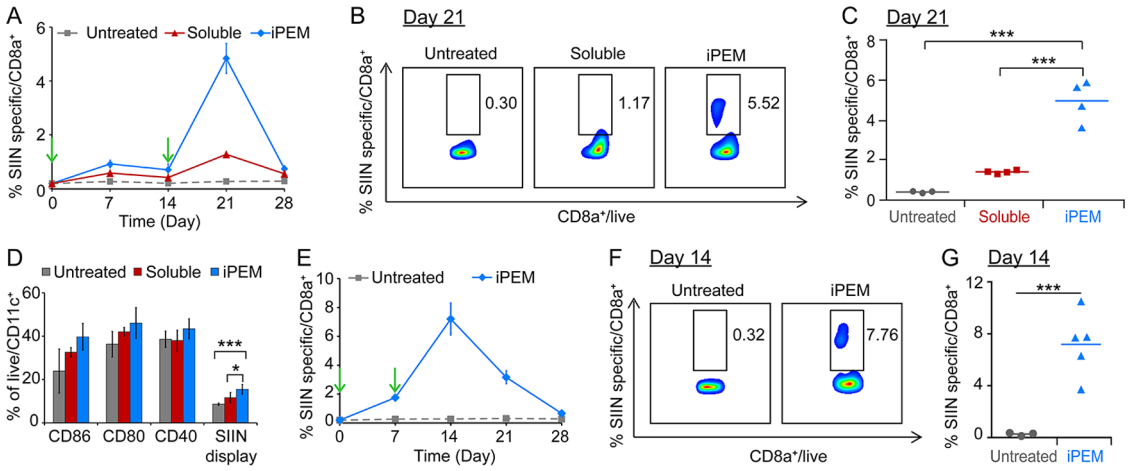

Figure 7. Immunization with (polyIC/SIIN*)$_2$ (iPEM) activates DCs and promotes efficient primary and secondary CD8$^+$ T cell responses in mice. (A) Development of SIINFEKL-specific CD8$^+$ T cells in peripheral blood over 28 days. Mice were immunized with iPEMs or soluble antigen and adjuvant on day 0 then boosted on day 14. (B) Representative scatter plots showing distributions of SIINFEKL$^+$ and CD8$^+$ T cells on day 21. (C) Statistical analysis of antigen-specific T cell response in each group on day 21. (D) Activation and SIIN presentation by DCs in the draining LNs of mice 3 days after priming immunizations with the indicated vaccines. (E) Development of SIINFEKL-specific CD8$^+$ T cells in peripheral blood over 28 days. Mice were immunized with iPEMs or soluble antigen and adjuvant on day 0 then boosted on day 7. (F) Representative scatter plots showing distributions of SIINFEKL$^+$ and CD8$^+$ T cells on day 14. (G) Statistical analysis of antigen-specific T cell response in each group on day 14.

AuNP-(polyIC/SIIN*)$_2$ presented SIIN compared to 0.1 ± 0.05% of cells treated with AuNP-(polyIC/CTRL)$_2$ (Figure 5E). The levels of antigen presentation induced by AuNP-(polyIC/SIIN*)$_2$ were similar to those observed in cells treated with equivalent doses of soluble polyIC and SIIN (92.0 ± 0.8%) but significantly greater than the baseline levels observed in DCs treated with uncoated AuNPs, LPS, or polyIC—none of which contained SIIN (Figure 5E). As with activation, the degree of presentation could be controlled by changing the number of layers used to build iPEMs (Supporting Information Figure S4D). Further, antigen presentation was also selective, as the frequency of SIIN presentation in DCs treated with AuNP-(polyIC/CTRL)$_2$ was equivalent to the levels observed in other samples that did not contain SIIN (Figure 5E). Thus, iPEMs deliver peptide antigens to DCs in a manner that can be efficiently processed and specifically presented through key pathways involved in cell-mediated immunity (*e.g.*, MHC-I).

iPEM-Coated AuNPs Drive Antigen-Specific T Cell Proliferation and Effector Cytokine Secretion. We next tested if DCs that process iPEMs can activate and expand T cells specific for antigens used to assemble iPEMs. DCs were treated with iPEM-coated AuNPs for 48 h and then cocultured for 72 h with CFSE-labeled CD8$^+$ T cells (see Methods) from OT-I mice—a strain in which CD8$^+$ T cell receptors are responsive to SIINFEKL peptide presented in MHC-I. T cells cocultured with DCs treated with AuNP-(polyIC/SIIN*)$_2$ were highly proliferative (*i.e.*, high cell division and dye dilution) compared with T cells incubated with untreated DCs, DCs treated with an irrelevant control peptide (CTRL), and DCs incubated with uncoated AuNPs (*i.e.*, low cell division and dye dilution) (Figure 6A). These results were indicated by decreasing CFSE levels observed in each successive T cell generation in samples treated with AuNP-(polyIC/SIIN*)$_2$, as well as positive controls that included DCs treated with soluble SIIN or a mixture of soluble SIIN and polyIC (Figure 6A). Quantitative analysis of CFSE MFIs across all samples confirmed these trends, with AuNP-(polyIC/SIIN*)$_2$ causing low MFI values due to high levels of proliferation and samples with cells that did not proliferate exhibiting high MFI values for CFSE (Figure 6B). These findings were also reflected in frequency data (Figure 6C) evaluated using the gates shown in Figure 6A.

We next investigated whether iPEM-expanded T cells exhibit functional characteristics by quantifying inflammatory and effector cytokine levels in the supernatants of coculture samples. Figure 6D summarizes the secretion levels of interferon gamma (IFN-γ), tumor necrosis factor (TNF), and an early inflammatory cytokine associated with DCs and inflammasome actication, interleukin 1-beta (IL1-β). Cells treated with AuNP-(polyIC/SIIN*)$_2$ induced significant levels of both IFN-γ (Figure 6D, green bar) and TNF (Figure 6D, yellow bar) compared with cells treated with AuNP-(polyIC/CTRL)$_2$, untreated cells, and cells treated with either polyIC or SIIN peptide. These increased cytokine levels were similar to the high levels observed in cells treated with a mixture of soluble polyIC and SIIN. In contrast to the results for IFN-γ and TNF, the levels of IL-1β, a key component in the NALP3 inflammasome signaling cascade, were only slightly elevated in cells treated with AuNP-(polyIC/SIIN*)$_2$ (Figure 6D, blue bar). These levels were much lower than those observed in cells treated with LPS but similar to the near baseline levels measured in cells treated with soluble polyIC, soluble

SIIN, or both. Together, the data in Figure 5 and Figure 6 confirm that adjuvants used to assemble iPEMs selectively activate TLR pathways, providing the necessary signals to support processing and presentation of iPEM antigens by DCs. These effects drive antigen-specific T cell proliferation and effector cytokine secretion but do not induce a more generalized inflammatory cytokine associated with less specific inflammation (*e.g.*, inflammasomes).

Immunization with iPEM-Coated AuNPs Efficiently Expands Antigen-Specific T Cells in Mice. We next investigated the ability of iPEM-coated AuNPs to drive antigen-specific $CD8^+$ T cell responses in mice. In these studies, mice were immunized (i.d.) with peptide and polyIC vaccines formulated as simple mixtures or as iPEMs coated on AuNPs. Each week after the priming immunization (day 0), MHC-I SIINFEKL tetramer was used to enumerate the frequency of SIINFEKL-specific circulating $CD8^+$ T cells (Figure 7A). After 7 days, mice immunized with AuNP-(polyIC/SIIN*)$_2$ exhibited the highest frequency of SIINFEKL-specific $CD8^+$ T cells (0.92 $\pm$ 0.14%), compared with 0.58 $\pm$ 0.07% in mice immunized with a simple mixture, and 0.27 $\pm$ 0.02% in unimmunized mice (Figure 7A). These levels contracted over the following 7 days. To test recall response, mice were boosted on day 14 using the same respective formulation that each group received during the priming injection. One week post-boost, mice immunized with the iPEMs exhibited a potent and synergistic expansion of antigen-specific $CD8^+$ T cells (4.84 $\pm$ 0.56%) that was ~4-fold greater than the frequencies observed in mice immunized with a simple mixture (1.28 $\pm$ 0.04%) of polyIC and antigen (Figure 7B,C). T cells then contracted over 7 days, following kinetics consistent with a classic recall response.

To assess the mechanism behind the immunogenicity of iPEM-AuNPs, naïve mice were again immunized with either the iPEM vaccine or the simple mixture vaccine. After 3 days, draining LNs were excised and DC activation was measured. Mice receiving the iPEM vaccine exhibited modest increases in CD86 and CD80 expression compared with soluble vaccines, though these differences were only significant compared with levels observed in untreated mice (Figures 7D and S5). Interestingly, lymph-node-resident DCs in mice treated with iPEMs exhibited significant increases in SIINFEKL presentation *via* MHC-I (Figures 7D and S5) compared with mice immunized with the simple mixture or unvaccinated mice. Next we tested how T cell expansion kinetics would be altered by more frequent immunization. In this study, mice were primed as above then boosted on day 7 (Figure 7E–G), with weekly monitoring of antigen-specific T cell expansion in peripheral blood. Mice immunized with iPEM formulations drove striking levels of circulating, SIIN-specific $CD8^+$ T cells, with a mean frequency of 7.20 $\pm$ 1.11% and a maximum value or 10.50% (Figure 7F,G). This development was also rapid, occurring within 1 week after the booster injection. Taken together, these findings demonstrate that iPEMs coated on AuNPs enhance response to immune signals, driving more efficient antigen presentation and DC activation to promote potent increases in antigen-specific T cell expansion and recall.

DISCUSSION

We have developed a new type of PEM assembled entirely from immune signals to form iPEMs. These nanoscale coatings comprise peptide antigens and TLR agonists as adjuvants. iPEMs can be deposited on substrates at both macro- and nanolength scales, do not require solvents or mixing, and juxtapose antigens and adjuvants in the films in a manner that maintains the immunogenicity and selectivity of each component. Importantly, iPEM assembly does not require any other polymeric components. This is a new feature for the PEM field, as PEMs previously used in vaccination involve other polymers (*e.g.*, poly(methacrylic acid), hyaluronic acid, poly(styrenesulfonate), poly(allylamine hydrochloride), PAH, poly-L-arginine),[20,37] which can influence adaptive or innate immune response.[38] Thus, these new materials could improve rational design of future vaccines by eliminating the intrinsic immune effects associated with many polymeric materials used in PEMs and other biomaterials-based vaccines.

In first assembling iPEMs, we drew on past reports demonstrating that polyelectrolyte multilayers can be assembled from peptides, exhibiting stabilities that can be manipulated depending on the amino acid composition or charge of each residue.[11,39] Our initial attempts revealed that the zwitterionic nature of SIIN did not provide sufficient charge density to promote sustainable film growth (Figure 2A,B). Thus, we modified SIIN with a R_9 cationic anchor to form SIIN*. This modification resulted in linear growth of films assembled from polyIC and SIIN*, demonstrating a simple, modular method to quantitatively control the incorporation of each immune signal by adjusting the number of deposition steps (Figure 2B,C).

We extended iPEMs to injectable particles by leveraging the favorable properties of AuNPs as nontoxic, inert substrates for vaccine delivery. After coating, iPEMs maintained sizes useful for vaccination that ranged between ~50 and 200 nm, depending on the number of layers deposited. CryoTEM (Figure 3D) confirmed that iPEMs coated on AuNPs exhibited a core–shell structure consistent with growth indicated by oscillating surface charge (Figure 3B) and increasing diameter (Figure 3A). Although on planar substrates, each iPEM bilayer had a thickness of 10.1 nm (Figure 2A), the greater rate of growth on colloidal substrates (Figure 3A) may result from interaction between opposite, excess charges on a fraction of coated AuNPs. Such bridging effects could increase

the effective diameter and were observable in some particles during cyroTEM imaging (Figure 3D,ii and Supporting Information Figure S2A). Stability studies indicated that particles were stable in serum-free medium at elevated temperature, with no significant change in diameter over 24 h (Figure S2B). Under more stringent conditions where particles were incubated in serum-rich medium, size increased over 24 h to 200−300 nm, indicating that particles experience some aggregation in the presence of serum. However, these studies also demonstrate that iPEM-AuNPs maintain sizes useful for vaccination even in a challenging mimic of the physiologic environment.

Our studies (Figure 5A−C), and past reports,[29,40] demonstrate that uncoated AuNPs do not exhibit intrinsic properties that activate immune pathways. In contrast, many nondegradable and degradable polymers do elicit these responses. Some of the most relevant materials to our studies include common PEM components such as hyaluronic acid, poly(vinylpyrrolidone), and poly(methacrylic acid),[19,38] along with ubiquitous materials such as polystyrene and PLGA.[30,31] At least in part, the immunogenicity of many synthetic polymers results from activation of danger-associated molecular patterns (DAMPs) and pathogen-associated molecular patterns (PAMPs) signaling pathways such as inflammasomes.[30] Many of these innate inflammatory pathways are driven by IL-1β production, yet iPEMs coated on AuNPs did not induce this cytokine (Figure 6D), suggesting that these materials function more specifically (*e.g.*, TLR3 signaling).[41,42] Additionally, AuNPs can be synthesized with tunable well-defined diameters, support facile surface modification, and increase retention time of conjugated cargos (*e.g.*, peptides) in lymph nodes after injection.[43,44] Coupling PEMs with AuNPs thus takes advantage of the inert, well-controlled physiochemical properties of AuNPs while providing a simple means of controlling loading of one or multiple types of immune signals.

In DC uptake studies, we discovered that iPEMs co-deliver both antigen and adjuvant to DCs without toxicity (Figure 4). Interestingly, at low dilutions, we observed much more similar association levels between the peptide and polyIC signal, whereas at the highest dilutions, peptide association was markedly higher than the polyIC signal (Figure 4C). A few possibilities could account for these observations. First, polyIC is particularly susceptible to RNase nuclease activity at dilute concentrations, and RNA degradation could generate free dye molecules which leave the cell to lower the signal. At high concentrations (*i.e.*, low dilutions), it is also possible that sink conditions exist such that the fraction of polyIC degraded over the culture time is relatively small compared with the relative fraction degraded over the same interval when the starting concentration is 16-fold lower (*i.e.*, high dilution). Despite these factors, at higher concentrations, the levels were similar. This is an important finding since delivery of both an antigen and a stimulatory signal are required to activate danger/pathogen sensing pathways (*e.g.*, DAMPs, PAMPs) and generate adaptive immunity. Further, R_9 is a strong cell-penetrating peptide able to carry cargo across a cell membrane in an endocytosis-independent manner.[45−47] This molecule has previously been used to modify enzymes with low charge density to allow incorporation into PEMs when alternatingly assembled with synthetic polyanions and degradable polycations.[36] Thus, R_9 likely plays an additional role as a component that enhances the uptake of iPEMs by immune cells. Mechanistic studies are underway to isolate the contributions of R_9 to iPEM uptake and to test if any increases in uptake result from endocytosis-independent routes previously reported for R_9 and other CPPs (*e.g.*, penetratin, transportan).[47]

We also assessed several other important immunological characteristics of iPEMs by using primary cell coculture models. First, DCs treated with polyIC/SIIN* exhibited similar levels of surface activation markers compared to cells treated with equivalent doses of soluble polyIC and peptide (Figure 5A−C). This result indicates that the potency of immune signals (*i.e.*, antigen, adjuvant) used to assemble iPEMs is not impacted by incorporation into PEMs. With respect to adjuvant, iPEMs formulated with polyIC activated TLR3 signaling, while iPEMs assembled from antigen and C-ODN did not (Figure 5D). We also demonstrated that DCs treated with AuNP-(polyIC/SIIN*)$_2$ process SIIN*, resulting in presentation of SIIN peptide *via* the MHC-I (Figure 5E). We observed selectivity in these studies, as cells treated with iPEMs assembled with an irrelevant control peptide (CTRL) did not exhibit a signal corresponding to SIIN presentation following antibody staining (Figure 5E). Functionally, treatment of DCs with AuNP-(polyIC/SIIN*)$_2$ before coculture with OT-I T cells led to T cell expansion (Figure 6A−C) and secretion of key effector cytokines (Figure 6D). In particular, AuNP-(polyIC/SIIN*)$_2$ induced both IFN-γ and TNF secretion at levels that were much higher than those observed in wells treated with SIIN peptide or with AuNP-(polyIC/CTRL)$_2$ (Figure 6D). These cytokines are important mediators of adaptive immunity, supporting antiviral response, inflammation, and macrophage activation. Also, in this experiment, we observed proliferation of OT-I T cells when DCs were treated with SIIN peptide (Figure 6A−C), but these responses were not functional as indicated by the lack of cytokine secretion observed in SIIN-treated samples in Figure 6D. Together, these findings directly confirm that antigens used to assemble iPEMs are presented in a manner that expands T cells with cognate specificity for these antigens, leading to secretion of effector cytokines. Conversely, iPEMs containing adjuvants and irrelevant antigens, while able to activate DCs, do

not drive functional responses (*i.e.*, cytokine secretion) in T cells recognizing antigens that were not included during iPEM assembly.

We also discovered that iPEMs coated on AuNPs generate antigen-specific $CD8^+$ T cells responses in mice (Figure 7). Compared to soluble antigen and adjuvant, iPEM formulations enhance immune response, generating more potent immunity during both primary and recall responses. In mice, iPEMs greatly increase antigen presentation and generally enhance DC activation in draining lymph nodes. This enhancement may have resulted from specific features of iPEMs including the particulate nature and high signal density. Such characteristics generally facilitate better uptake and activation of antigen-presenting cells at injection sites or in draining lymph nodes. This idea was supported by *ex vivo* culture studies in which iPEMs were internalized at significantly higher levels than soluble peptide or adjuvant (Figure 4B–D). However, our studies with other iPEM architectures in Figure 5A–C (*e.g.*, AuNP-$(polyIC/CTRL)_2$, AuNP-$(C\text{-}ODN/SIIN^*)_2$) indicated that—at least in cell culture—simply formulating peptide into iPEMs did not enhance immunogenicity. Further, the finding that both AuNP-$(polyIC/CTRL)_2$ and AuNP-$(polyIC/SIIN^*)_2$ drove similar levels of activation indicates that the contribution from adjuvants used to assemble iPEMs is generalizable to different antigens. Thus, juxtaposition of the antigen and adjuvant in iPEMs likely plays an important role in increasing the frequency of cells encountering and processing both the antigen and adjuvant, a requirement for generation of adaptive immune response. In contrast, none of these features are present in the soluble mixtures of antigen and adjuvant. The synergistic increase in recall response upon boosting may also hint at polarization of immune function induced by iPEMs, for example, biasing toward T cell memory. Future studies to investigate this possibility could shed light onto how iPEM components are processed to drive or bias T cell differentiation. Other follow-on studies will involve assembly of iPEMs with clinically relevant antigens, building on our current studies that demonstrate the potential of iPEMs as a modular platform to promote antigen-specific $CD8^+$ T cells.

CONCLUSIONS

In this paper, we have developed a new vaccine platform for rationally designing PEM coatings from immune signals. This is the first time PEMs have been assembled in a way that eliminates potentially confounding intrinsic properties of synthetic polymers or other structural components often included in PEM films. iPEM-coated AuNPs activate antigen-presenting cells and elicit antigen-specific immune responses from T cells in culture and in mice. Future studies to investigate the molecular mechanism of adjuvanticity (*e.g.*, TLR signaling) and the functional utility of expanded T cells in clinically relevant disease models will help identify opportunities for iPEM coatings to be harnessed in tailoring the development of specific immune responses. Ultimately, this platform could contribute to new vaccines that allow more rational control over the specific characteristics of the immune responses that are generated.

METHODS

Materials. Peptides from ovalbumin (SIINFEKL, SIIN; SIINFEKL-R_9; SIIN*) or an irrelevant control peptide from myelin oligodendrocyte glycoprotein (MOG_{35-55}-R_9; referred to as CTRL in text and figures) were synthesized by Genscript. All peptides were at least 98% pure and were synthesized with or without a fluorescein (FITC) tag. LPS (TLR4) was purchased from Life Technologies (Invitrogen). PolyIC (TLR3) and Pam3CSK4 (TLR2) were purchased from Invivogen. Non-immunostimulatory control oligonucleotide (referred to as C-ODN in text and figures) was synthesized by Integrated DNA Technologies and had a sequence of TCCTGAGCTTGAAGT (ODN 2088 control). Polyethylenimine (PEI, MW = 50 000) and poly(sodium 4-styrenesulfonate) (MW = 70 000) were from Sigma. PolyIC was labeled with Cy5 using a Label IT Cy5 labeling kit (Mirus Bio LLC). (4′,6-Diamidino-2-phenylindole) (DAPI), wheat germ agglutinin Texas Red conjugate, and paraformaldehyde (4%) were from Life Technologies. Gold(III) chloride trihydrate (99.9%), chitosan (MW = 2000), and phosphate buffered saline (PBS, 1×) were from Sigma. $CD11c^+$ positive isolation beads were from Miltenyi Biotec. EasySep mouse $CD8^+$ isolation kits and spleen dissociation medium was from STEMCELL Technologies. All ELISA antibodies and reagents were from BD Biosciences. Antibodies for CD80 (FITC), CD86 (PE-Cy7), CD40 (PE), and SIINFEKL presented in MHC-I were from BD Biosciences or Biolegend. RPMI cell culture medium was from MP Biomedicals. C57BL/6J (B6) and C57BL/6-Tg (TcraTcrb, 1100Mjb/J) (OT-I) mice were from The Jackson Laboratory.

Cells and Animals. All animal research and care was carried out in accordance with local, state, and federal regulations and under guidelines approved by the University of Maryland IACUC. For primary cell studies, spleens were isolated from 4–8 week old female mice and processed to a single cell suspension. For studies involving CD11c-purified DCs, splenic DCs from B6 mice were then purified from the cell suspensions by positive isolation according to the manufacturer's instructions. $CD8^+$ T cells were isolated from OT-I mice by negative selection according to the manufacturer's instructions. Splenocytes, isolated DCs, or isolated T cells were then cultured under 5% CO_2 in RPMI medium containing 10% fetal bovine serum, penicillin (100 units/mL), and streptomycin (100 μg/mL), HEPES (10 mM), L-glutamine (2 mM), 2-mercaptoethanol (55 μM), nonessential amino acids (1×).

Assembly and Characterization of iPEMs on Planar Substrate. Silicon (Silicon Inc.) and quartz (VWR) substrates were cut into 15 mm × 5 mm sections using a diamond dicing saw (model 1006, Micro Automation). Substrates were cleaned with acetone, methanol, and deionized (DI) water and then dried under filtered and compressed air. Cleaned substrates were treated with oxygen plasma (March Jupiter III) for 3 min to provide a charged surface for layer-by-layer assembly of a precursor PEM layer of $(PEI/PSS)_1$, similar to previous reports.[36,48,49] Substrates were then immersed in either SIIN or SIIN* solution (500 μg/mL in DI water) for 5 min, followed by immersion in DI water for 30 s. The substrates were then immersed in polyIC solution (500 μg/mL in DI water) for 5 min, followed by an

additional 30 s wash in DI water. These steps were repeated until the desired number of bilayers was deposited. For experiments with fluorescently labeled film components, the procedure was identical but polyIC was replaced with Cy5-labeled polyIC and SIIN/SIIN* was replaced with FITC-labeled peptide. Film thicknesses were measured by ellipsometry (Gaertner Scientific) on iPEM-coated silicon substrates, with average values calculated from at least five areas for each substrate. UV−vis spectrophotometry (Thermo Scientific) was used to measure the absorbance of iPEMs on quartz chips with wavelengths of 260 and 488 nm, respectively, for polyIC and FITC-labeled peptides.

AuNP Synthesis and Characterization. Synthesis protocols for AuNP templates were adapted from previous literature.[50,51] Briefly, 50 mL of chitosan solution (0.3%, w/v) in 1% acetic acid was heated to 100 °C and mixed with 40 μL aqueous chloroauric acid ($HAuCl_4$, 0.01 M). The solution was maintained at 100 °C for 25 min to obtain a red colored dispersion.

Assembly and Characterization of PEMs on AuNPs. AuNPs were coated with PEMs using an alternating deposition process similar to the process used for planar substrates and in past reports involving coating of PEMs onto colloidal substrates.[34] Briefly, 1.9 mg of AuNP was collected by centrifugation (13500 rcf, 15 min) and resuspended 100 μL of DI water. AuNPs were then added to 900 μL of polyIC solution (500 μg/mL in DI water), mixed by pipetting, and placed in a sonic water bath for 45 s at room temperature. The suspension was maintained for 5 min, collected by centrifugation at 4 °C (12 500 rcf, 15 min), and then washed with DI water to obtain AuNP-polyIC$_1$. Following centrifugation and resuspension in a fresh aliquot of 100 μL of DI water, polyIC-coated AuNPs were incubated with 900 μL of peptide SIIN* (500 μg/mL) and washed as above to obtain AuNP-(polyIC/SIIN*)$_1$. These steps were repeated until the desired numbers of layers of each component were deposited. In some studies, peptides and polyIC were replaced with fluorescently labeled versions using FITC for peptides and Cy5 for polyIC. Loading of polyIC and peptides on AuNPs was characterized by UV−vis absorbance of deposition solutions using the Beer−Lambert law at a wavelength of 260 nm for polyIC and standard curves prepared at 488 nm for FITC-labeled peptides. Uncoated AuNPs or iPEM-AuNPs were imaged by cryogenic transmission electron microscopy (JEOL JEM 2100) at 100 kV and a temperature of −170 °C. The sizes of PEM-modified AuNPs were measured by dynamic light scattering using a Zetasizer Nano Z analyzer. Values reported are mean diameters ± standard deviation based on intensity measurements. Stability studies were carried out by incubating iPEM-coated AuNPs (0.85 mg/mL) in RPMI 1640 or RPMI 1640 + 5% fetal bovine serum (FBS) at 37 °C. At each indicated time point, dynamic light scattering was used to measure particle size distributions. Because serum-rich medium exhibits inherent scattering from serum proteins on the order of tens of nanometers, control measurements using serum-rich medium without addition of iPEMs were used as a baseline. iPEMs (AuNP-(polyIC/SIIN*)$_2$) were then added to the serum-rich medium. The appearance of a new, non-overlapping peak corresponding to iPEM-AuNPs was observed, and software integration was used to analyze the size and standard deviation of the iPEM peak (based on intensity).

Cell Internalization Studies. Association and uptake of coated AuNPs by DCs was characterized by flow cytometry (FACS Cantoll, BD Bioscience) and confocal microscopy (Leica SP5X). For flow cytometry, CD11c$^+$ splenic DCs were seeded in 96-well plates at a concentration of 1.0×10^5 cells per well. Uncoated AuNPs or AuNP-(polyIC-Cy5/SIIN*-FITC)$_2$ were then added to each well in a volume of 25 μL. Two-fold serial dilutions were performed using a starting iPEM/AuNP concentration of 1.9 mg/mL. Cells were then cultured for 16 h. After incubation, cells were washed twice by centrifugation and resuspended in FACS buffer (PBS + 1% BSA). The washed cells were finally resuspended in a DAPI solution (0.1% in PBS + 1% BSA) to allow assessment of viability by flow cytometry (*i.e.*, DAPI$^-$ cells). Cells positive for FITC and Cy5 signals compared with negative controls were considered to have associated with iPEMs.

Confocal microscopy was used to confirm cell internalization by incubating 10 μL (1.9×10^{-2} mg) of uncoated AuNPs or AuNPs coated with (polyIC-Cy5/SIIN*-FITC)$_2$ with 6.0×10^6 DCs in 25 mm dishes with glass coverslip inlays. After 4 h, the cells were gently washed two times with PBS to remove the free iPEM-coated AuNPs. Cells were then fixed with 4% paraformaldehyde for 15 min at 37 °C and washed twice with PBS. Cell membranes were stained with a wheat germ agglutinin Texas Red conjugate (5 μg/mL in PBS) at room temperature for 10 min protected from light. The cells were then washed with PBS, resuspended in Hoescht stain, and imaged by confocal microscopy under a 63× oil immersion objective. Individual image channels were collected for DAPI (nuclei), FITC (peptide), Texas Red (cell membrane), and Cy5 (polyIC) and then merged and analyzed using CellSens, ImageJ, and Adobe Creative Cloud.

DC Activation and Antigen Presentation. For DC activation and antigen presentation studies, CD11c$^+$ splenic B6 DCs were stimulated with AuNPs coated with 0−3 bilayers of polyIC (or C-ODN) and each peptide for 24 h. Untreated cells or cells treated with LPS (1 μg/mL), polyIC (10 μg/mL), C-ODN (10 μg/mL), AuNPs (1.9×10^{-2} mg/well), SIIN peptide (5 μg/mL), or CTRL peptide (5 μg/mL) were used as controls. After incubation with iPEM-coated AuNPs, DCs were washed twice with PBS + 1% BSA and then blocked in anti-CD16/CD32 (Fcγ III/II receptor) (25× dilution, BD Biosciences) for 15 min at room temperature. The cells were then stained with antibodies for CD80 (FITC), CD86 (AmCyan-A), and CD40 (PE). To quantify presentation of SIINFEKL *via* the MHC-I pathway, cells were stained with a PE-Cy7-labeled antibody (BioLegend) against anti-mouse H-2Kb bound to OVA257-264 (SIINFEKL). All antibodies were fluorescent conjugates and were used by staining for 20 min at a 1:300 dilution in PBS + 1% BSA. Cells were then washed twice in PBS + 1% BSA and resuspended in a DAPI solution for analysis by flow cytometry. The data analysis was performed with Flowjo (Treestar).

TLR3 Signaling. TLR3 activity was assessed using HEK-Blue mTLR3 cells (Invivogen). Cells were seeded at a concentration of 5.0×10^4 cells per well, followed by treatment with Pam3CSK4 (0.2 μg/mL), LPS (1.0 μg/mL), polyIC (10 μg/mL), C-ODN (5 μg/mL), SIIN peptide (5 μg/mL), AuNPs (1.9×10^{-2} mg/well), AuNP-(C-ODN/SIIN*)$_2$ (80 μg/mL), or AuNP-(polyIC/SIIN*)$_2$ (80 μg/mL). After 16 h, the absorbance was read at 625 nm using a UV/vis platereader (Molecular Devices).

T Cell Coculture, Activation, and Proliferation. CD11c$^+$ B6 splenocytes were treated with AuNPs (uncoated or iPEM-coated), LPS (1 μg/mL), polyIC (10 μg/mL), AuNPs (1.9×10^{-2} mg/well), SIIN peptide (5 μg/mL), control peptide (CTRL, 5 μg/mL), or soluble polyIC (10 μg/mL) + SIIN (5 μg/mL). Untreated cells were used as a negative control. After 48 h, T cells isolated from OT-I mice were stained with CellTrace CFSE cell proliferation reagent (5 μg/mL in cell culture medium) by incubation at room temperature for 5 min. T cells were then cocultured with each DC sample by addition of 3.0×10^5 T cells per well. After an additional 48 h of incubation, cells were centrifuged (800 rcf for 5 min), the supernatants were collected for ELISA, and the cells were washed in PBS + 1% FBS. Cells were then blocked as above and stained with anti-CD8a (APC) for 15 min at room temperature. Lastly, cells were washed twice and resuspended in DAPI. T cell proliferation was determined by the mean fluorescence intensity of the CFSE signal among DAPI$^-$ and CD8$^+$ cells compared with positive and negative controls.

ELISA. Cytokine levels in the supernatants collected from DCs/T cell cocultures were analyzed by ELISA using mouse TNF, IFN-γ, and IL-1β ELISA reagents (BD Bioscience) according to the manufacturer's instructions. Ten microliters of each supernatant was used in each test, and cytokine concentrations were quantified by comparison to standard curves prepared from known standards.

***In Vivo* Immunization Studies.** For *in vivo* studies, B6 mice in groups of five were unimmunized or injected intradermally on each flank (i.d., 25 μL) with either vaccine formulation (*i.e.*, soluble, AuNP-(polyIC/SIIN*)$_2$) containing equivalent doses of antigen (32.5 μg) or adjuvant (52.0 μg). Mice were primed at day 0 and, in some studies, received a booster injection on either day 7 or day 14. For *in vivo* activation and antigen presentation studies, mice were injected with either vaccine formulation (*i.e.*, soluble, AuNP-(polyIC/SIIN*)$_2$). After 3 days, mice were euthanized, and the inguinal lymph nodes were collected and then

processed to a single cell suspension by passage through a cell strainer (40 μm). Cells were blocked and stained as above before analysis by flow cytometry.

***In Vivo* Analysis of Antigen-Specific CD8$^+$ T Cell Expansion.** During immunization studies, peripheral blood was collected from mice at day 0, 7, 14, 21, and 28. The blood samples were treated with 1 mL of ACK lysing buffer (Life Technologies) for 5 min, collected by centrifugation (800*g*, 5 min), treated with ACK a second time, and washed in PBS before collection. Blocking was next carried out as described above. Cells were then stained with SIINFEKL MHC-I tetramer (PE conjugate) for 30 min using a 25× dilution and for CD8a (APC conjugate) as described above. The stained cells were washed and resuspended in DAPI and analyzed by flow cytometry.

Statistical Analysis. One-way ANOVA with a Tukey post-test was performed using Graphpad Prism (version 6.02) for statistical testing. *P* values of <0.05 (*), <0.01 (**), and <0.001 (***) were used to indicate statistical significance. Data are reported as mean values ± standard error of the mean. All experiments were conducted using replicates of four samples (*e.g.*, cell culture wells) or animal group sizes of 3−5 mice per group. Data shown in all figures are representative examples of 2−4 experiments with similar results.

Conflict of Interest: The authors declare no competing financial interest.

Supporting Information Available: Absorbance spectra used to determine cargo loading, flow cytometry histograms used to determine dendritic cell activation levels during *in vitro* and *in vivo* studies, and dendritic cell activation and antigen presentation levels as a function of the number of layers used to construct iPEMs. The Supporting Information is available free of charge on the ACS Publications website at DOI: 10.1021/acsnano.5b02153.

Acknowledgment. We thank the University of Maryland Nanoscale Imaging Spectroscopy and Properties (NISP) Lab for assistance with cryoTEM, and A. Beaven at the University of Maryland Imaging Core Facility for assistance with confocal microscopy. This work was supported in part by NSF CAREER Award No. 1351688 and the Pharmaceutics division of the PhRMA Foundation. C.M.J. is a Damon Runyon-Rachleff Innovator supported by the Damon Runyon Foundation, a Young Investigator supported by the Alliance for Cancer Gene Therapy, and a Young Investigator supported by the Melanoma Research Alliance. L.H.T. is a fellow supported by the NSF Graduate Research Fellowship Program Grant No. DGE1322106.

REFERENCES AND NOTES

1. Zinkernagel, R. M.; Ehl, S.; Aichele, P.; Oehen, S.; Kundig, T.; Hengartner, H. Antigen Localisation Regulates Immune Responses in a Dose- and Time-Dependent Fashion: A Geographical View of Immune Reactivity. *Immunol. Rev.* **1997**, *156*, 199–209.
2. Mueller, S. N.; Germain, R. N. Stromal Cell Contributions to the Homeostasis and Functionality of the Immune System. *Nat. Rev. Immunol.* **2009**, *9*, 618–629.
3. Irvine, D. J.; Swartz, M. A.; Szeto, G. L. Engineering Synthetic Vaccines Using Cues from Natural Immunity. *Nat. Mater.* **2013**, *12*, 978–990.
4. Swartz, M. A.; Hirosue, S.; Hubbell, J. A. Engineering Approaches to Immunotherapy. *Sci. Transl Med.* **2012**, *4*, 148rv9.
5. Andorko, J. I.; Hess, K. L.; Jewell, C. M. Harnessing Biomaterials To Engineer the Lymph Node Microenvironment for Immunity or Tolerance. *AAPS J.* **2015**, *17*, 323–338.
6. Decher, G. Fuzzy Nanoassemblies: Toward Layered Polymeric Multicomposites. *Science* **1997**, *277*, 1232–1237.
7. Jewell, C. M.; Lynn, D. M. Multilayered Polyelectrolyte Assemblies as Platforms for the Delivery of DNA and Other Nucleic Acid-Based Therapeutics. *Adv. Drug Delivery Rev.* **2008**, *60*, 979–999.
8. De Koker, S.; De Cock, L. J.; Rivera-Gil, P.; Parak, W. J.; Velty, R. A.; Vervaet, C.; Remon, J. P.; Grooten, J.; De Geest, B. G. Polymeric Multilayer Capsules Delivering Biotherapeutics. *Adv. Drug Delivery Rev.* **2011**, *63*, 748–761.
9. Yan, Y.; Bjonmalm, M.; Caruso, F. Assembly of Layer-by-Layer Particles and Their Interactions with Biological Systems. *Chem. Mater.* **2014**, *26*, 452–460.
10. Jaber, J. A.; Schlenoff, J. B. Recent Developments in the Properties and Applications of Polyelectrolyte Multilayers. *Curr. Opin. Colloid Interface Sci.* **2006**, *11*, 324–329.
11. Haynie, D. T.; Zhang, L.; Zhao, W.; Rudra, J. S. Protein-Inspired Multilayer Nanofilms: Science, Technology and Medicine. *Nanomed. Nanotechnol.* **2006**, *2*, 150–157.
12. Wang, Q.; Schlenoff, J. B. Single- and Multicompartment Hollow Polyelectrolyte Complex Microcapsules by One-Step Spraying. *Adv. Mater.* **2015**, *27*, 2077–2082.
13. Elbakry, A.; et al. Layer-by-Layer Coated Gold Nanoparticles: Size-Dependent Delivery of DNA into Cells. *Small* **2012**, *8*, 3847–3856.
14. Zhang, P. P.; Qiao, Y.; Wang, C. M.; Ma, L. Y.; Su, M. Enhanced Radiation Therapy with Internalized Polyelectrolyte Modified Nanoparticles. *Nanoscale* **2014**, *6*, 10095–10099.
15. DeMuth, P. C.; Min, Y. J.; Huang, B.; Kramer, J. A.; Miller, A. D.; Barouch, D. H.; Hammond, P. T.; Irvine, D. J. Polymer Multilayer Tattooing for Enhanced DNA Vaccination. *Nat. Mater.* **2013**, *12*, 367–376.
16. DeMuth, P. C.; Min, Y.; Irvine, D. J.; Hammond, P. T. Implantable Silk Composite Microneedles for Programmable Vaccine Release Kinetics and Enhanced Immunogenicity in Transcutaneous Immunization. *Adv. Healthcare Mater.* **2014**, *3*, 47–58.
17. Cui, J. W.; De Rose, R.; Best, J. P.; Johnston, A. P. R.; Alcantara, S.; Liang, K.; Such, G. K.; Kent, S. J.; Caruso, F. Mechanically Tunable, Self-Adjuvanting Nanoengineered Polypeptide Particles. *Adv. Mater.* **2013**, *25*, 3468–3472.
18. Chong, S. F.; Sexton, A.; De Rose, R.; Kent, S. J.; Zelikin, A. N.; Caruso, F. A Paradigm for Peptide Vaccine Delivery Using Viral Epitopes Encapsulated in Degradable Polymer Hydrogel Capsules. *Biomaterials* **2009**, *30*, 5178–5186.
19. Sexton, A.; Whitney, P. G.; Chong, S. F.; Zelikin, A. N.; Johnston, A. P. R.; De Rose, R.; Brooks, A. G.; Caruso, F.; Kent, S. J. A Protective Vaccine Delivery System for *in Vivo* T Cell Stimulation Using Nanoengineered Polymer Hydrogel Capsules. *ACS Nano* **2009**, *3*, 3391–3400.
20. De Geest, B. G.; et al. Polymeric Multilayer Capsule-Mediated Vaccination Induces Protective Immunity against Cancer and Viral Infection. *ACS Nano* **2012**, *6*, 2136–2149.
21. Connor, E. E.; Mwamuka, J.; Gole, A.; Murphy, C. J.; Wyatt, M. D. Gold Nanoparticles Are Taken up by Human Cells but Do Not Cause Acute Cytotoxicity. *Small* **2005**, *1*, 325–327.
22. Khlebtsov, N.; Dykman, L. Biodistribution and Toxicity of Engineered Gold Nanoparticles: A Review of *in Vitro* and *in Vivo* Studies. *Chem. Soc. Rev.* **2011**, *40*, 1647–1671.
23. Parveen, S.; Misra, R.; Sahoo, S. K. Nanoparticles: A Boon to Drug Delivery, Therapeutics, Diagnostics and Imaging. *Nanomed. Nanotechnol.* **2012**, *8*, 147–166.
24. Gribova, V.; Auzely-Velty, R.; Picart, C. Polyelectrolyte Multilayer Assemblies on Materials Surfaces: From Cell Adhesion to Tissue Engineering. *Chem. Mater.* **2012**, *24*, 854–869.
25. Niikura, K.; et al. Gold Nanoparticles as a Vaccine Platform: Influence of Size and Shape on Immunological Responses *in Vitro* and *in Vivo*. *ACS Nano* **2013**, *7*, 3926–3938.
26. Reddy, S. T.; van der Vlies, A. J.; Simeoni, E.; Angeli, V.; Randolph, G. J.; O'Neill, C. P.; Lee, L. K.; Swartz, M. A.; Hubbell, J. A. Exploiting Lymphatic Transport and Complement Activation in Nanoparticle Vaccines. *Nat. Biotechnol.* **2007**, *25*, 1159–1164.
27. Almeida, J. P. M.; Figueroa, E. R.; Drezek, R. A. Gold Nanoparticle Mediated Cancer Immunotherapy. *Nanomed. Nanotechnol.* **2014**, *10*, 503–514.
28. Yeste, A.; Nadeau, M.; Burns, E. J.; Weiner, H. L.; Quintana, F. J. Nanoparticle-Mediated Codelivery of Myelin Antigen and a Tolerogenic Small Molecule Suppresses Experimental Autoimmune Encephalomyelitis. *Proc. Natl. Acad. Sci. U. S.A.* **2012**, *109*, 11270–11275.

29. Moyano, D. F.; Goldsmith, M.; Solfiell, D. J.; Landesman-Milo, D.; Miranda, O. R.; Peer, D.; Rotello, V. M. Nanoparticle Hydrophobicity Dictates Immune Response. *J. Am. Chem. Soc.* **2012**, *134*, 3965–3967.
30. Sharp, F. A.; et al. Uptake of Particulate Vaccine Adjuvants by Dendritic Cells Activates the Nalp3 Inflammasome. *Proc. Natl. Acad. Sci. U.S.A.* **2009**, *106*, 870–875.
31. Demento, S. L.; et al. Inflammasome-Activating Nanoparticles as Modular Systems for Optimizing Vaccine Efficacy. *Vaccine* **2009**, *27*, 3013–3021.
32. Hotaling, N. A.; Cummings, R. D.; Ratner, D. M.; Babensee, J. E. Molecular Factors in Dendritic Cell Responses to Adsorbed Glycoconjugates. *Biomaterials* **2014**, *35*, 5862–5874.
33. Mayya, K. S.; Schoeler, B.; Caruso, F. Preparation and Organization of Nanoscale Polyelectrolyte-Coated Gold Nanoparticles. *Adv. Funct Mater.* **2003**, *13*, 183–188.
34. Schneider, G.; Decher, G. From Functional Core/Shell Nanoparticles Prepared via Layer-by-Layer Deposition to Empty Nanospheres. *Nano Lett.* **2004**, *4*, 1833–1839.
35. Bishop, C. J.; Tzeng, S. Y.; Green, J. J. Degradable Polymer-Coated Gold Nanoparticles for Co-delivery of DNA and SiRNA. *Acta Biomater.* **2015**, *11*, 393–403.
36. Jewell, C. M.; Fuchs, S. M.; Flessner, R. M.; Raines, R. T.; Lynn, D. M. Multilayered Films Fabricated from an Oligoarginine-Conjugated Protein Promote Efficient Surface-Mediated Protein Transduction. *Biomacromolecules* **2007**, *8*, 857–863.
37. De Rose, R.; Zelikin, A. N.; Johnston, A. P. R.; Sexton, A.; Chong, S. F.; Cortez, C.; Mulholland, W.; Caruso, F.; Kent, S. J. Binding, Internalization, and Antigen Presentation of Vaccine-Loaded Nanoengineered Capsules in Blood. *Adv. Mater.* **2008**, *20*, 4698.
38. Park, J.; Gerber, M. H.; Babensee, J. E. Phenotype and Polarization of Autologous T Cells by Biomaterial-Treated Dendritic Cells. *J. Biomed. Mater. Res., Part A* **2015**, *103*, 170–184.
39. Zhang, L.; Haynie, D. T. Internal Structure of Wet and Dry Polypeptide Multilayer Nanofilms. *Biomacromolecules* **2007**, *8*, 2033–2037.
40. Safari, D.; et al. Gold Nanoparticles as Carriers for a Synthetic Streptococcus Pneumoniae Type 14 Conjugate Vaccine. *Nanomed. Nanotechnol.* **2012**, *7*, 651–662.
41. Martinon, F.; Mayor, A.; Tschopp, J. The Inflammasomes: Guardians of the Body. *Annu. Rev. Immunol.* **2009**, *27*, 229–265.
42. Neumann, S.; Burkert, K.; Kemp, R.; Rades, T.; Rod Dunbar, P.; Hook, S. Activation of the Nlrp3 Inflammasome Is Not a Feature of All Particulate Vaccine Adjuvants. *Immunol. Cell Biol.* **2014**, *92*, 535–542.
43. Lin, A. Y.; Almeida, J. P.; Bear, A.; Liu, N.; Luo, L.; Foster, A. E.; Drezek, R. A. Gold Nanoparticle Delivery of Modified Cpg Stimulates Macrophages and Inhibits Tumor Growth for Enhanced Immunotherapy. *PLoS One* **2013**, *8*, e63550.
44. Cobaleda-Siles, M.; et al. An Iron Oxide Nanocarrier for Dsrna to Target Lymph Nodes and Strongly Activate Cells of the Immune System. *Small* **2014**, *10*, 5054–5067.
45. Deshayes, S.; Morris, M. C.; Divita, G.; Heitz, F. Cell-Penetrating Peptides: Tools for Intracellular Delivery of Therapeutics. *Cell. Mol. Life Sci.* **2005**, *62*, 1839–1849.
46. Walrant, A.; et al. Different Membrane Behaviour and Cellular Uptake of Three Basic Arginine-Rich Peptides. *Biochim. Biophys. Acta* **2011**, *1808*, 382–393.
47. Copolovici, D. M.; Langel, K.; Eriste, E.; Langel, U. Cell-Penetrating Peptides: Design, Synthesis, and Applications. *ACS Nano* **2014**, *8*, 1972–1994.
48. Jewell, C. M.; Zhang, J. T.; Fredin, N. J.; Lynn, D. M. Multilayered Polyelectrolyte Films Promote the Direct and Localized Delivery of DNA to Cells. *J. Controlled Release* **2005**, *106*, 214–223.
49. Jewell, C. M.; Zhang, J.; Fredin, N. J.; Wolff, M. R.; Hacker, T. A.; Lynn, D. M. Release of Plasmid DNA from Intravascular Stents Coated with Ultrathin Multilayered Polyelectrolyte Films. *Biomacromolecules* **2006**, *7*, 2483–2491.
50. Huang, H. Z.; Yang, X. R. Synthesis of Chitosan-Stabilized Gold Nanoparticles in the Absence/Presence of Tripolyphosphate. *Biomacromolecules* **2004**, *5*, 2340–2346.
51. Bhumkar, D. R.; Joshi, H. M.; Sastry, M.; Pokharkar, V. B. Chitosan Reduced Gold Nanoparticles as Novel Carriers for Transmucosal Delivery of Insulin. *Pharm. Res.* **2007**, *24*, 1415–1426.